Single-step electrodeposition of superhydrophobic black NiO thin films

Ahmad Bahramian, Marielle Eyraud, F. Vacandio, V. Hornebecq, T. Djenizian, P. Knauth

Single step electrodeposition of superhydrophobic black NiO thin films

A. Bahramian[a], M. Eyraud[a]*, F. Vacandio[a], V. Hornebecq[a], T. Djenizian[b], P. Knauth[a]

[a] Aix Marseille Univ, CNRS, Madirel, UMR 7246, Electrochemistry of Materials Group, Campus St Jérôme, 13013 Marseille, France

[b] Mines Saint-Etienne, Center of Microelectronics in Provence, Department of Flexible Electronics, 13541 Gardanne, France

* Corresponding author: marielle.eyraud@univ-amu.fr

Highlights

- Electrodeposition of superhydrophobic black NiO films on Cu is studied.
- Superhydrophobicity is attributed to the formation of a rough surface.
- An improvement of the corrosion resistance of Cu sub-layers is observed.

Abstract

Black finished surfaces have extensive applications in many domains, such as optics, solar cells, and aerospace. The single step electrodeposition of superhydrophobic black NiO films from a dimethyl sulfoxide based electrolyte is described in this paper. The physicochemical properties of the obtained film were characterized using Scanning Electron Microscopy, X-ray Diffraction, and electrochemical tests (Electrochemical Impedance Spectroscopy and potentiodynamic polarization). A rough surface with a low reflection of light was formed after the deposition process that increased the contact angle of water from about 87º (for bare Cu) to 163º (in presence of the black coating), which improved the corrosion resistance of the Cu substrate by about 30%. The formed black NiO film revealed a notably high stability and kept its appearance even after corrosion tests.

Keywords: Black NiO, Superhydrophobic, Corrosion, Electrodeposition, thin films

1. Introduction

Black finished surfaces are useful for optical instruments, solar cells, black decorative coatings, and for defense and aerospace industries [1,2]. There are several studies regarding black finished surfaces, including black Si, black Cr, and black Ni [2–4]. Black Ni surfaces are normally obtained by etching a low P content Ni-P (1-4 wt.% P) in an oxidizing acid [5,6]. Etching forms several cracks on the surface of the Ni-P film. These cracks, providing multiple reflection and absorption sites for incident light, are responsible for the black aspect of the surface [7]. However, the film also becomes very vulnerable to corrosion due to these cracks

[1]. Furthermore, blackening the surface by chemical etching induces a huge material loss that is not economical [8].

The corrosion of metals can be effectively blocked by decreasing the contact of the surface with the corrosive media. Superhydrophobic materials, i.e. surfaces with a water contact angle larger than 150º [9], reduce the corrosion, because the contact between the oxidizing media and the surface of the sample is reduced. Therefore, superhydrophobic films are known to offer an outstanding corrosion resistance [10–12]. Superhydrophobic films also offer self-cleaning, anti-fouling, and frost prevention properties. Superhydrophobicity can be obtained by modification of a surface owing to the surface energy decrease and the formation of a rough hierarchical surface morphology [13].

NiO is formed by oxidation at the surface of Ni-P during chemical etching. NiO is a p-type semi-conducting oxide with a fcc crystalline structure exhibiting a good chemical stability [14,15]. Several methods including annealing [17], sol-gel chemistry [18], ionic layer adsorption and reaction (SILAR) [19], and electrodeposition [20] have been investigated to form NiO. Electrodeposition has various advantages such as the ability to coat large surfaces, a homogenous deposition, a controllable morphology and thickness, high adhesion to the substrate, and few problems related to inter-diffusion [20]. Koussi *et al.* [20] have successfully electrodeposited NiO from a dimethyl sulfoxide (DMSO) based electrolyte. The mechanism of the electrodeposition of NiO in DMSO was described by the following equations in the absence (1) and in the presence of a low content of water (2), respectively:

$$Ni^{2+} + O^{2-} \rightarrow NiO \qquad (1)$$

$$Ni^{2+} + 2OH^{-} \rightarrow Ni(OH)_2 \rightleftharpoons NiO + H_2O \qquad (2)$$

In this paper, we report for the first time the single-step electrodeposition of a black superhydrophobic NiO coating from a DMSO-based electrolyte. The coating was characterized using Scanning Electron Microscopy (SEM), grazing incidence X-Ray Diffraction (grazing XRD), Water Contact Angle measurements (WCA), Electrochemical Impedance Spectroscopy (EIS) and potentiodynamic polarization tests.

2. Experimental procedure

The electrodeposition electrolyte was a DMSO based solution at 50°C, containing 190 $g.L^{-1}$ $NiSO_4$. $6H_2O$, 10 $g.L^{-1}$ $NiCl_2$. $6H_2O$, 8 $g.L^{-1}$ H_3PO_3, 16 $g.L^{-1}$ H_3BO_3, and 5 $mL.L^{-1}$ H_3PO_4. All the chemicals, provided by Sigma-Aldrich, were highly pure and used as received.

Cyclic voltammetry and potentiostatic electrodeposition experiments were performed with a potentiostat/galvanostat (VersaSTAT 3). Before the deposition, the Cu substrate was pre-treated according to reference [21]. A common 3-electrode setup was used consisting of the Cu substrate as working electrode, a Pt plate as counter electrode, and an Ag/AgCl (KCl saturated) as reference electrode. For cyclic voltammetry tests, the potential was gradually decreased from 0 V vs. the reference electrode, to -1.5 V and then increased to 0 V. The scan rate was 20 $mV.s^{-1}$. The electrodeposition was achieved by chronoamperometry. A constant potential of - 1V *vs.* the reference electrode was applied on the working electrode for 1200 s, while the solution was stirred with a speed of 650 rpm.

Two scanning electron microscopes (Philips XL 30 ESEM, and CARL ZEISS/Ultra 55) were used to study the surface and cross-section morphologies, respectively. The chemical composition of the films was investigated by Energy Dispersive Spectroscopy (EDS).

The sample reflectance was recorded using an UV−visible spectrophotometer (Varian Cary 300) equipped with an integrating sphere DRA-CA-30I in the 380−800 nm range. Measurements were performed 4 times for each sample by rotating the sample holder in order to probe the whole surface of the samples.

A Siemens D5000 diffractometer was employed to investigate the crystalline structure. XRD patterns were obtained over the 2θ range of 30–60° (with 0.04° step size) using Cu Kα radiation (λ = 0.15406 nm) generated at 30 mA and 40 kV.

A tensiometer (Adimec MX12P) was used to do the water contact angle measurements (2 µL droplets) at five different locations. Drop analysis LB-ADSA plugin in ImageJ software was used to measure the contact angle [22].

The corrosion resistance of the films was studied after 60 minutes immersion in a 3% NaCl solution by EIS and Tafel tests. The EIS measurements were done at Open Circuit Potential (OCP) in a frequency range from 100 kHz to 10 mHz with 10 mV peak-to-peak voltage amplitude. Zview was used to analyze the obtained EIS data. Potentiodynamic polarization experiments were carried out at a scan rate

of 0.5 mV/s from -300 mV (vs. OCP) to 500 mV (vs. reference electrode). The results were normalized by the exposed area to the corrosive media.

3. Results and Discussion

- Cathodic electrodeposition

The cyclic voltammetry curves of the cathodic electrodeposition of Ni from the DMSO based electrolyte are presented in Figure 1. It can be seen that the current density at -1 V is relatively low. Such a low value makes it kinetically favorable for the nucleation and growth to occur at preferential sites. Such type of 3D "island" growth (described by the Volmer-Weber model) is known to form a rough deposit. Figure 2 depicts the current density during the deposition of the film in DMSO at -1 V. The current density for NiO deposition from DMSO is notably lower than previously reported for Ni deposition from an aqueous electrolyte [21]. This observation points to the higher resistivity and lower throwing power in DMSO than in aqueous electrolytes, leading to a reduced deposition rate.

- Surface and cross-section morphology

Figure 3 shows the surface and cross-section morphologies of the black coating. In Figure 3A, the black appearance of the coating is obvious. The SEM image presents a surface made of several hierarchical island shape features that are regularly distributed over the surface. Such a morphology (that is similar to the known lotus leave morphology [23]) highly decreases the light reflection (Figure 4) and thus makes the surface look black. The increase in the reflection of the Cu substrate at around 550 nm is due to the natural color of Cu. Moreover, such a morphology offers a high roughness that increases the water contact angle (see below). The cross-section shows several well-distributed nanometric island shape features on the surface. Moreover, the formed black film was notably adhesive, since no cracks or delamination was observed at the interface between Cu and the coating.

- Chemical composition and structure

The chemical composition of the film is summarized in Table 1. A film composed of a mixture of NiO and Ni-P is formed on pure Cu. The high Cu content is due to the low thickness of the black film. The presence of S and C in the chemical composition is due to the incorporation of DMSO inside the film [20].

Figure 5 shows the grazing incidence XRD pattern of the black film. The strong sharp peak at 43.5 º is attributed to the NiO (200) reflection (NiO presents a NaCl-type structure) [14,16] that shows the preferential growth of the film. The absence of Ni peaks can be attributed to the amorphous nature of the Ni-P film. The average grain size D was estimated to be around 100 nm using the Debye Scherrer formula [14],

$$D = \frac{0.9\lambda}{\beta cos\theta} \quad (3)$$

where λ is the X-ray wavelength, β is the full width at half maximum of the peak, and θ is the diffraction angle. The grain size of the black film is notably bigger than that previously reported elsewhere [14,16,24]. The formation of bigger grains might be related to the low deposition rate from DMSO.

- Water contact angle

The water contact angle of the Cu substrate and the black film are shown in Figure 6. The contact angle values for the Cu substrate and the film were 83 ± 6º and 161 ± 3º, respectively. Therefore, applying the black NiO film changed the hydrophilic Cu surface to a superhydrophobic surface.

The hydrophobicity of these films was previously found to be due to the roughness of the surface [25]. The superhydrophobicity of the surface comes from the heterogeneous wetting, which means that the trapped air prevents the liquid from penetration [26]. This can be expressed by the following equation:

$$cos\,\theta^* = f(1 + cos\,\theta) - 1 \quad (4)$$

Where f is the area fraction of the droplet in contact with the solid (and thus 1-f is the area fraction of the droplet in contact with the trapped air), and θ^* and θ are the contact angles of the rough coating and the substrate (or flat surface). The f value calculated for the black NiO film is 0.049: it has a very low wetting ability, notably lower than some previously reported values for superhydrophobic Ni films (0.25 [27], and 0.13 [28]).

- Corrosion resistance

A typical impedance spectrum of the black NiO film is depicted in Figure 7. The film presents one time constant in its EIS data. The Randles model, which is the typical model to fit the EIS data of electrodeposited superhydrophobic NiO films [12,25,29], was employed to analyze the black NiO film. A Constant Phase

Element (CPE) was used to describe the non-ideal behavior of the interface. The impedance of a CPE is defined as:

$$Z_{CPE} = \frac{1}{Y_0(i\omega)^n} \quad (5)$$

Y_0 is the constant of admittance, i is the imaginary unit, ω is the angular frequency, and n is the CPE exponent [30]. n is also sometimes considered as the roughness factor since it is affected by the surface roughness [31]. The analyzed data of the black NiO film and Cu substrate (that is reported in [21]) are presented in Table 2. Note that the Cu substrate had an extra Warburg element in its equivalent circuit that expressed the diffusion-limitation of corrosion. The value of n for the Cu substrate and the black NiO film were 0.80 and 0.76, respectively. The n value for the substrate is low due to the presence a Warburg element. This observation is pointing out that the black NiO has a rougher surface. The modulus Y° is higher than the value expected for a "metallic" electrode. Rough surfaces have a higher specific capacitance than flat ones, and increasing the roughness of thin films will enhance their capacitance [32]. Moreover, electrodeposited NiO has been shown to have a high pseudocapacitance, useful for supercapacitor applications [33–35], attributed to some contribution of chemical capacitances.

Applying the thin black NiO film increased the corrosion resistance by about 25% (8.1 vs. 6.1 kΩ.cm^2 for NiO and Cu, respectively).

Figure 8 shows the polarization curves performed on the black NiO film and the bare Cu substrate. The Tafel extrapolation method was used in a potential range of ± 250 mV around OCP, to obtain the corrosion potential (E_{corr}), corrosion current density (i_{corr}), and anodic and cathodic slopes (β_a and β_c). The Stern-Geary equation was used to calculate the polarization resistance [36]. Table 3 summarizes these data for the black NiO film.

$$R_P = \frac{\beta_a \beta_c}{2.303(\beta_a + \beta_c) i_{corr}} \quad (6)$$

In comparison with the reported data for the Cu substrate [21], the black NiO film notably shifted the corrosion potential (+155 mV) to more anodic regions. This means a significant decrease in corrosion inclination [37]. The polarization resistance (6.4 and 9.5 kΩ for Cu and black NiO, respectively) shows about 33% increase, in good agreement with EIS results. The black NiO coating presents especially a lower current density at high potentials showing its high chemical stability.

Figure 9 shows that the surface morphology of the black NiO after the corrosion tests is clearly unchanged. The chemical composition of the surface after the corrosion tests is presented in Table 1. A comparison of the chemical composition of the black NiO film before and after the corrosion tests reveals that the amount of O increased, while the content of Ni decreased. A part of the Ni of Ni-P was dissolved, so the surface was enriched with other components (i.e. O and S), in agreement with the common corrosion mechanism of Ni films [37]. Therefore, the superhydrophobicity of the electrodeposited black NiO film strengthens the chemical stability and substantially improves the corrosion resistance.

4. Conclusions

The single step electrodeposition of superhydrophobic black NiO coatings from a DMSO based electrolyte is presented in this paper. A very rough surface containing many well-distributed island shaped features is formed that decreases the light reflection and increases the water contact angle.

The corrosion resistance increases by about 30% due to the superhydrophobicity of the surface that limits the contact between the surface and corrosive media. The effect of the deposition parameters on the properties of the black NiO film and the possibility to form it on other substrates, such as Al or Ti, is interesting for aerospace applications and will be the subject of a future study.

Acknowledgment

The project (APODISE, No. ANR-11-IDEX-0001-02) leading to this publication has received funding from Excellence Initiative of Aix-Marseille University - A*MIDEX, a French “Investissements d'Avenir” programme.

References

[1] Y. Liu, D. Beckett, D. Hawthorne, Effect of heat treatment, top coatings and conversion coatings on the corrosion properties of black electroless Ni–P films, Applied Surface Science. 257 (2011) 4486–4494. doi:10.1016/j.apsusc.2010.12.105.

[2] S. Somasundaram, A.M. Pillai, A. Rajendra, A.K. Sharma, High emittance black nickel coating on copper substrate for space applications, Journal of Alloys and Compounds. 643 (2015) 263–269. doi:10.1016/j.jallcom.2015.04.149.

[3] M.J. Persky, Review of black surfaces for space-borne infrared systems, Review of Scientific Instruments. 70 (1999) 2193–2217. doi:10.1063/1.1149739.

[4] T. Rahman, R.S. Bonilla, A. Nawabjan, P.R. Wilshaw, S.A. Boden, Passivation of all-angle black surfaces for silicon solar cells, Solar Energy Materials and Solar Cells. 160 (2017) 444–453. doi:10.1016/j.solmat.2016.10.044.
[5] Y.F. Wang, W.G. Fu, M. Feng, X.W. Cao, Investigation of the structure and the physical properties of nickel-phosphorus ultra-black surfaces, Applied Physics A. 90 (2008) 549–553. doi:10.1007/s00339-007-4323-z.
[6] P.P. Yue, Y.Z. Jin, X.D. Hu, H.Y. Yan, G.Q. Zeng, Study on the Surface Morphologies of Nickel-Phosphorus Ultra-Black Films, Advanced Materials Research. 924 (2014) 166–169. doi:10.4028/www.scientific.net/AMR.924.166.
[7] F. Xing, B. Zhao, W. Shi, Study on tunable fabrication of the ultra-black Ni–P film and its blacking mechanism, Electrochimica Acta. 100 (2013) 157–163. doi:10.1016/j.electacta.2013.03.145.
[8] R.J.C. Brown, P.J. Brewer, M.J.T. Milton, The physical and chemical properties of electroless nickel–phosphorus alloys and low reflectance nickel–phosphorus black surfaces, J. Mater. Chem. 12 (2002) 2749–2754. doi:10.1039/B204483H.
[9] T. Liu, S. Chen, S. Cheng, J. Tian, X. Chang, Y. Yin, Corrosion behavior of super-hydrophobic surface on copper in seawater, Electrochimica Acta. 52 (2007) 8003–8007. doi:10.1016/j.electacta.2007.06.072.
[10] Y. Wan, M. Chen, W. Liu, X. Shen, Y. Min, Q. Xu, The research on preparation of superhydrophobic surfaces of pure copper by hydrothermal method and its corrosion resistance, Electrochimica Acta. 270 (2018) 310–318. doi:10.1016/j.electacta.2018.03.060.
[11] D. Yu, J. Tian, J. Dai, X. Wang, Corrosion resistance of three-layer superhydrophobic composite coating on carbon steel in seawater, Electrochimica Acta. 97 (2013) 409–419. doi:10.1016/j.electacta.2013.03.071.
[12] S. Esmailzadeh, S. Khorsand, K. Raeissi, F. Ashrafizadeh, Microstructural evolution and corrosion resistance of super-hydrophobic electrodeposited nickel films, Surface and Coatings Technology. 283 (2015) 337–346. doi:10.1016/j.surfcoat.2015.11.005.
[13] Y. He, W.T. Sun, S.C. Wang, P.A.S. Reed, F.C. Walsh, An electrodeposited Ni-P-WS 2 coating with combined super-hydrophobicity and self-lubricating properties, Electrochimica Acta. 245 (2017) 872–882. doi:10.1016/j.electacta.2017.05.166.
[14] Y. Akaltun, T. Çayır, Fabrication and characterization of NiO thin films prepared by SILAR method, Journal of Alloys and Compounds. 625 (2015) 144–148. doi:10.1016/j.jallcom.2014.10.194.
[15] M. Martínez-Gil, M.I. Pintor-Monroy, M. Cota-Leal, D. Cabrera-German, A. Garzon-Fontecha, M.A. Quevedo-López, M. Sotelo-Lerma, Influence of annealing temperature on nickel oxide thin films grown by chemical bath deposition, Materials Science in Semiconductor Processing. 72 (2017) 37–45. doi:10.1016/j.mssp.2017.09.021.
[16] M.R. Das, A. Mukherjee, P. Mitra, Structural, optical and ac electrical characterization of CBD synthesized NiO thin films: Influence of thickness, Physica E: Low-Dimensional Systems and Nanostructures. 93 (2017) 243–251. doi:10.1016/j.physe.2017.06.018.
[17] P. Horak, Z. Remes, V. Bejsovec, J. Vacik, S. Danis, M. Kormunda, Nickel oxide films by thermal annealing of ion-beam-sputtered Ni: Structure and electro-optical properties, Thin Solid Films. 640 (2017) 52–59. doi:10.1016/j.tsf.2017.08.047.
[18] M. Jlassi, I. Sta, M. Hajji, H. Ezzaouia, Optical and electrical properties of nickel oxide thin films synthesized by sol–gel spin coating, Materials Science in Semiconductor Processing. 21 (2014) 7–13. doi:10.1016/j.mssp.2014.01.018.
[19] S.U. Mutkule, S.T. Navale, V.V. Jadhav, S.B. Ambade, M. Naushad, A.D. Sagar, V.B. Patil, F.J. Stadler, R.S. Mane, Solution-processed nickel oxide films and their liquefied petroleum gas sensing activity, Journal of Alloys and Compounds. 695 (2017) 2008–2015. doi:10.1016/j.jallcom.2016.11.037.

[20] S. Koussi-Daoud, A. Planchat, A. Renaud, Y. Pellegrin, F. Odobel, T. Pauporté, Solvent-Templated Electrodeposition of Mesoporous Nickel Oxide Layers for Solar Cell Applications, ChemElectroChem. 4 (2017) 2618–2625. doi:10.1002/celc.201700495.
[21] A. Bahramian, M. Eyraud, F. Vacandio, P. Knauth, Improving the corrosion properties of amorphous Ni-P thin films using different additives, Surface and Coatings Technology. 345 (2018) 40–52. doi:10.1016/j.surfcoat.2018.03.075.
[22] A.F. Stalder, T. Melchior, M. Müller, D. Sage, T. Blu, M. Unser, Low-bond axisymmetric drop shape analysis for surface tension and contact angle measurements of sessile drops, Colloids and Surfaces A: Physicochemical and Engineering Aspects. 364 (2010) 72–81. doi:10.1016/j.colsurfa.2010.04.040.
[23] Y. Liu, S. Li, J. Zhang, Y. Wang, Z. Han, L. Ren, Fabrication of biomimetic superhydrophobic surface with controlled adhesion by electrodeposition, Chemical Engineering Journal. 248 (2014) 440–447. doi:10.1016/j.cej.2014.03.046.
[24] S.R. Nalage, M.A. Chougule, S. Sen, P.B. Joshi, V.B. Patil, Sol–gel synthesis of nickel oxide thin films and their characterization, Thin Solid Films. 520 (2012) 4835–4840. doi:10.1016/j.tsf.2012.02.072.
[25] M. Hashemzadeh, K. Raeissi, F. Ashrafizadeh, S. Khorsand, Effect of ammonium chloride on microstructure, super-hydrophobicity and corrosion resistance of nickel coatings, Surface and Coatings Technology. 283 (2015) 318–328. doi:10.1016/j.surfcoat.2015.11.008.
[26] P. Esmaeilzadeh, M.T. Sadeghi, Z. Fakhroueian, A. Bahramian, R. Norouzbeigi, Wettability alteration of carbonate rocks from liquid-wetting to ultra gas-wetting using TiO 2 , SiO 2 and CNT nanofluids containing fluorochemicals, for enhanced gas recovery, Journal of Natural Gas Science and Engineering. 26 (2015) 1294–1305. doi:10.1016/j.jngse.2015.08.037.
[27] T. Hang, A. Hu, H. Ling, M. Li, D. Mao, Super-hydrophobic nickel films with micro-nano hierarchical structure prepared by electrodeposition, Applied Surface Science. 256 (2010) 2400–2404. doi:10.1016/j.apsusc.2009.10.074.
[28] F. Tian, A. Hu, M. Li, D. Mao, Superhydrophobic nickel films fabricated by electro and electroless deposition, Applied Surface Science. 258 (2012) 3643–3646. doi:10.1016/j.apsusc.2011.11.130.
[29] S. Khorsand, K. Raeissi, F. Ashrafizadeh, M.A. Arenas, A. Conde, Corrosion behaviour of super-hydrophobic electrodeposited nickel–cobalt alloy film, Applied Surface Science. 364 (2016) 349–357. doi:10.1016/j.apsusc.2015.12.122.
[30] E. Huttunen-Saarivirta, P. Rajala, M. Bomberg, L. Carpén, EIS study on aerobic corrosion of copper in ground water: influence of micro-organisms, Electrochimica Acta. 240 (2017) 163–174. doi:10.1016/j.electacta.2017.04.073.
[31] S.M. Rezaei Niya, M. Hoorfar, On a possible physical origin of the constant phase element, Electrochimica Acta. 188 (2016) 98–102. doi:10.1016/j.electacta.2015.11.142.
[32] S. Torabi, M. Cherry, E.A. Duijnstee, V.M. Le Corre, L. Qiu, J.C. Hummelen, G. Palasantzas, L.J.A. Koster, Rough Electrode Creates Excess Capacitance in Thin-Film Capacitors, ACS Applied Materials & Interfaces. 9 (2017) 27290–27297. doi:10.1021/acsami.7b06451.
[33] A.I. Inamdar, Y. Kim, S.M. Pawar, J.H. Kim, H. Im, H. Kim, Chemically grown, porous, nickel oxide thin-film for electrochemical supercapacitors, Journal of Power Sources. 196 (2011) 2393–2397. doi:10.1016/j.jpowsour.2010.09.052.
[34] U.M. Patil, R.R. Salunkhe, K.V. Gurav, C.D. Lokhande, Chemically deposited nanocrystalline NiO thin films for supercapacitor application, Applied Surface Science. 255 (2008) 2603–2607. doi:10.1016/j.apsusc.2008.07.192.
[35] K.-C. Liu, M.A. Anderson, Porous Nickel Oxide/Nickel Films for Electrochemical Capacitors, J. Electrochem. Soc. 143 (1996) 7.
[36] T. Pojtanabuntoeng, B. Kinsella, H. Ehsani, J. McKechnie, Assessment of corrosion control by pH neutralisation in the presence of glycol at low temperature, Corrosion Science. 126 (2017) 94–103. doi:10.1016/j.corsci.2017.06.018.

[37] G. Liu, Z. Huang, L. Wang, W. Sun, S. Wang, X. Deng, Effects of Ce4+ on the structure and corrosion resistance of electroless deposited Ni–Cu–P coating, Surface and Coatings Technology. 222 (2013) 25–30. doi:10.1016/j.surfcoat.2013.01.053.

Tables

Table 1. Chemical composition of the black coating before and after corrosion tests

Element	Before corrosion tests: Wt.%	After corrosion tests: Wt.%
C	3.6	3.2
O	11.0	13.9
P	2.6	2.8
S	7.8	8.8
Ni	61.8	56.2
Cu	13.2	15.1

Table 2. EIS fit values of the black NiO film and Cu substrate

Sample	R_s ($\Omega.cm^2$)	CPE_{dl}		R_{ct} ($k\Omega.cm^2$)	W		
		Q ($\mu F.cm^{-2}.s^{n-1}$)	n		W-R ($k\Omega.cm^2$)	W-T s	W-P
Black NiO	7.5	578.2	0.76	8.1	-	-	-
Cu Sub. [21]	20.3	129.8	0.80	0.02	6.1	165.9	0.43

Table 3. Corrosion current density, corrosion potential, anodic and cathodic slopes, and polarization resistance of the black NiO film

Sample	i_{corr} ($\mu A.cm^{-2}$)	E_{corr} (mV) vs. Ag/AgCl	Average Tafel slope (mV. dec^{-1})		R_p ($k\Omega.cm^2$)
			β_a	β_c	
Black NiO	1.64	-45	44	149	9.5
Cu Sub. [21]	3.32	-200	66	195	6.4

Figures

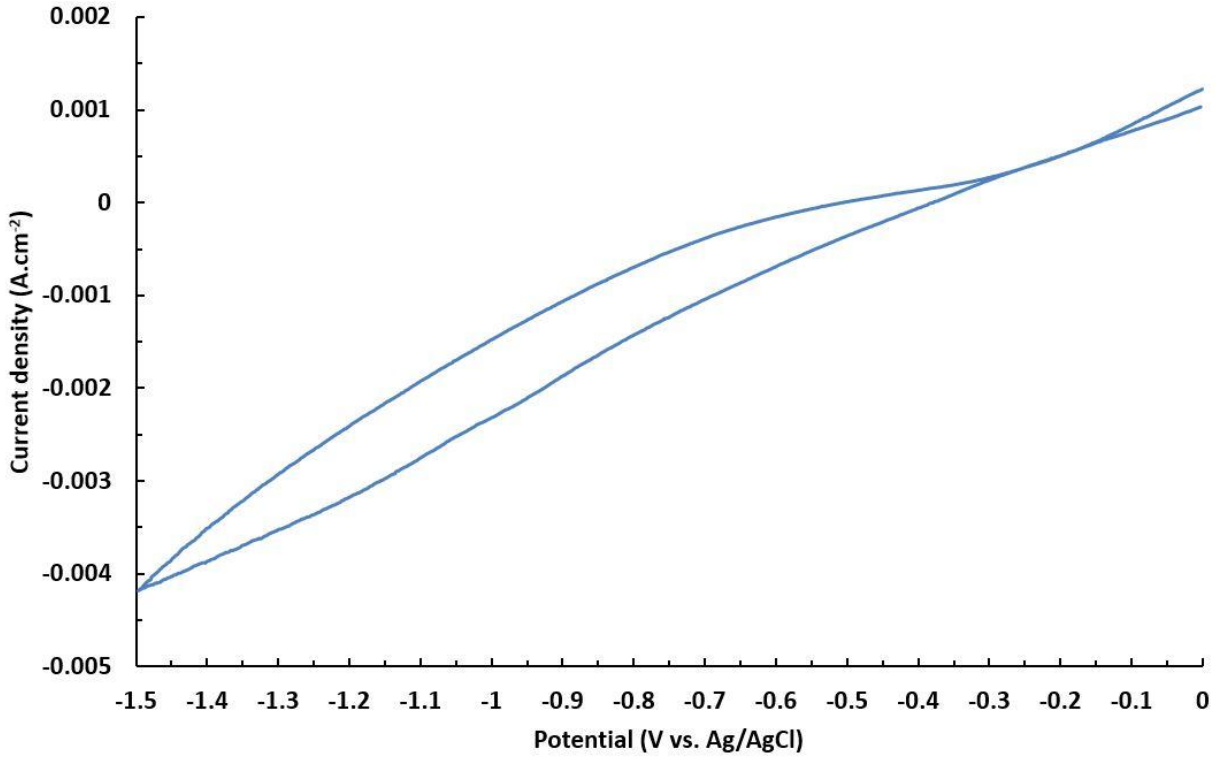

Figure 1. CV curve for the cathodic electrodeposition of Ni from the DMSO based electrolyte on Cu with a scan rate of 20 mV.s^{-1}.

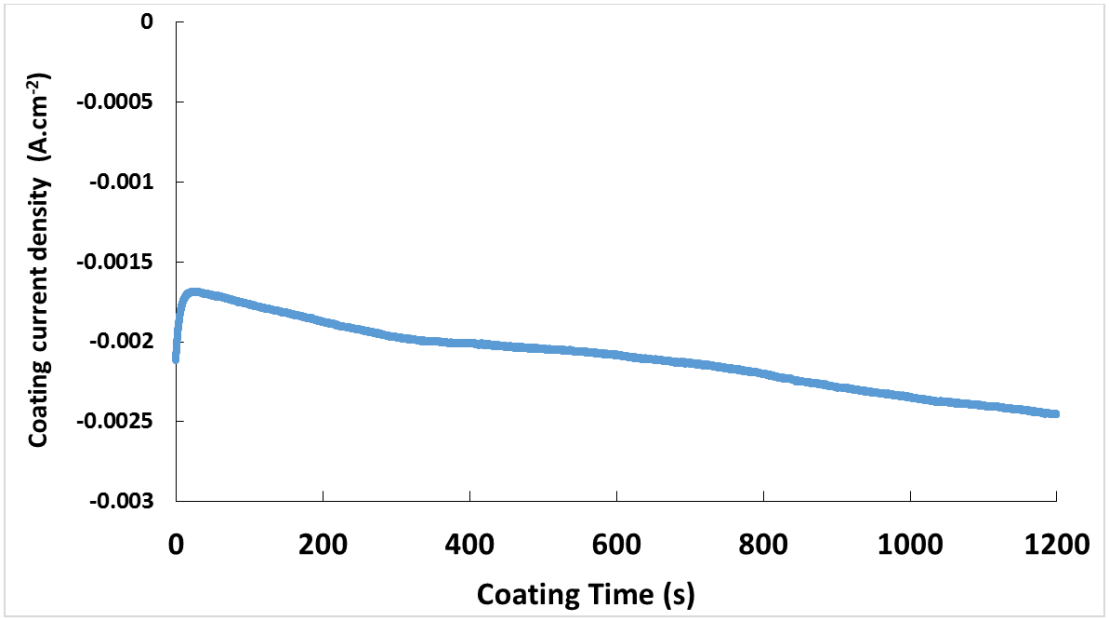

Figure 2. Current density as a function of the coating time for a black NiO film obtained in DMSO.

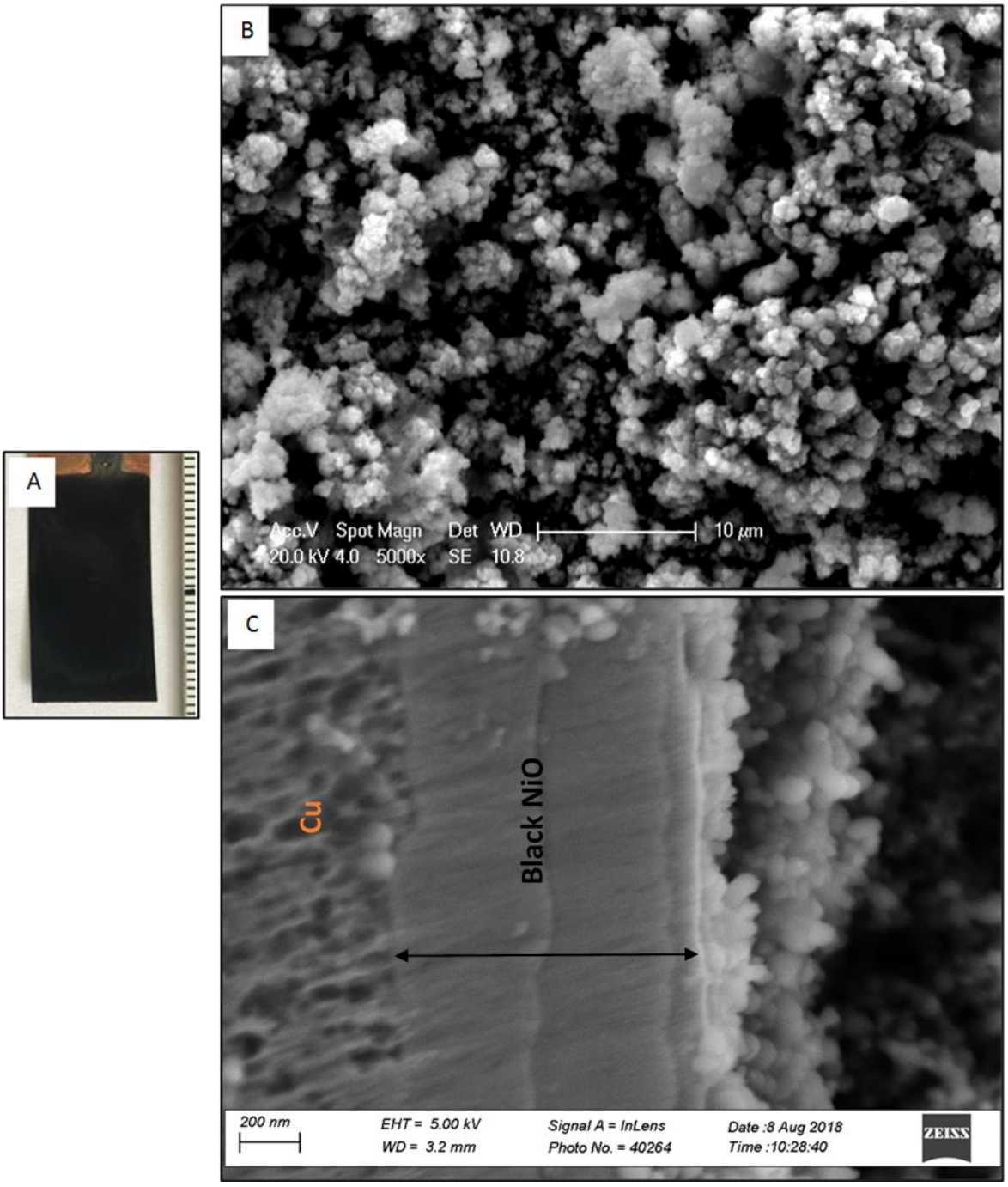

Figure 3. (A) Black NiO film on Cu and its surface (B) and cross-section (C) morphology.

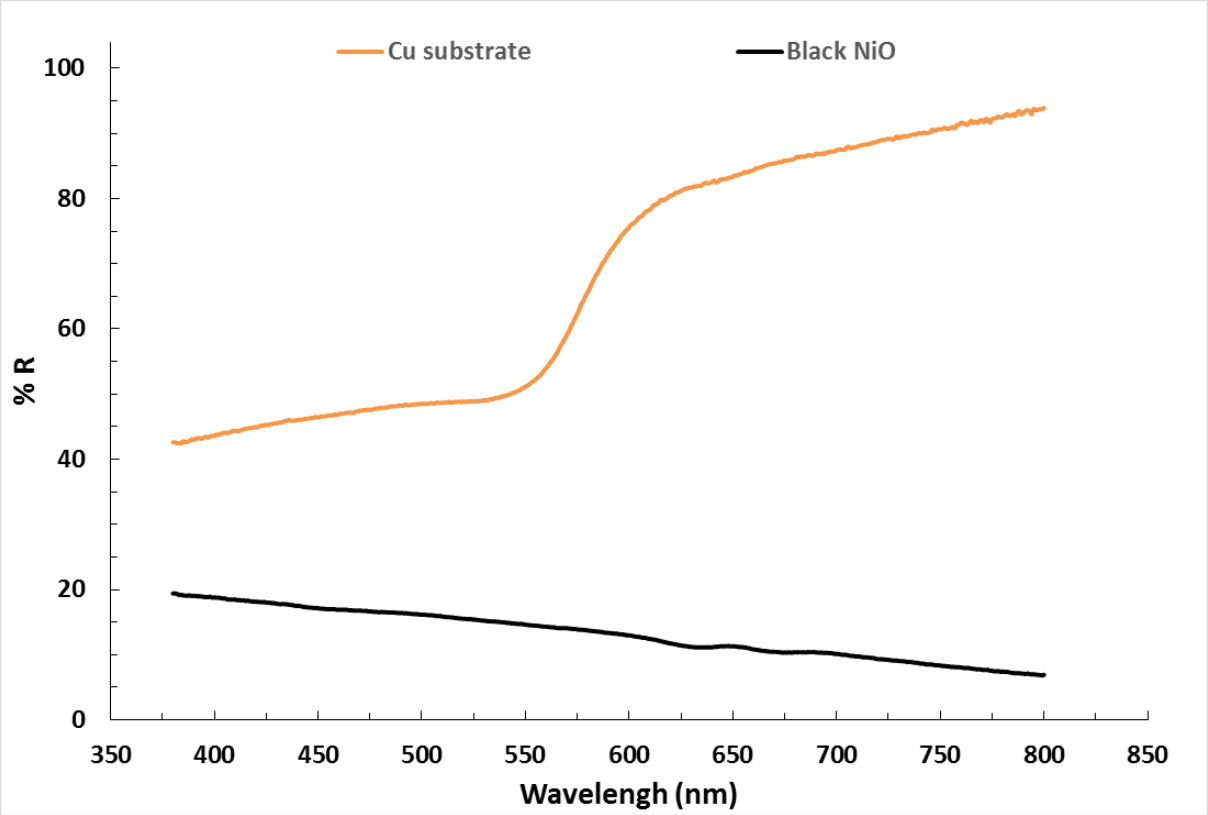

Figure 4. Reflectance of Cu substrate and black NiO film as a function of the wavelength of light.

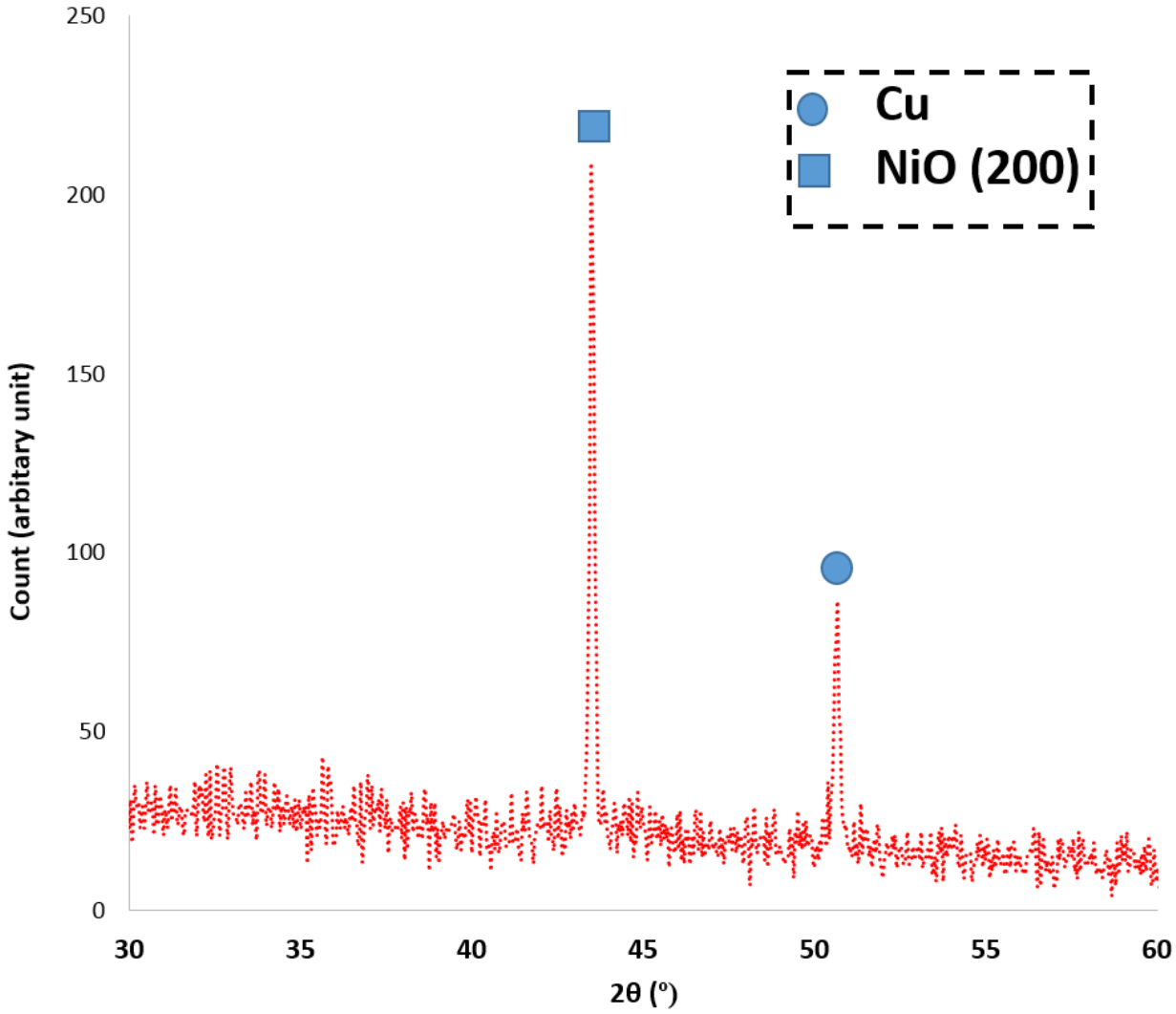

Figure 5. Grazing incidence XRD pattern of the black NiO coating.

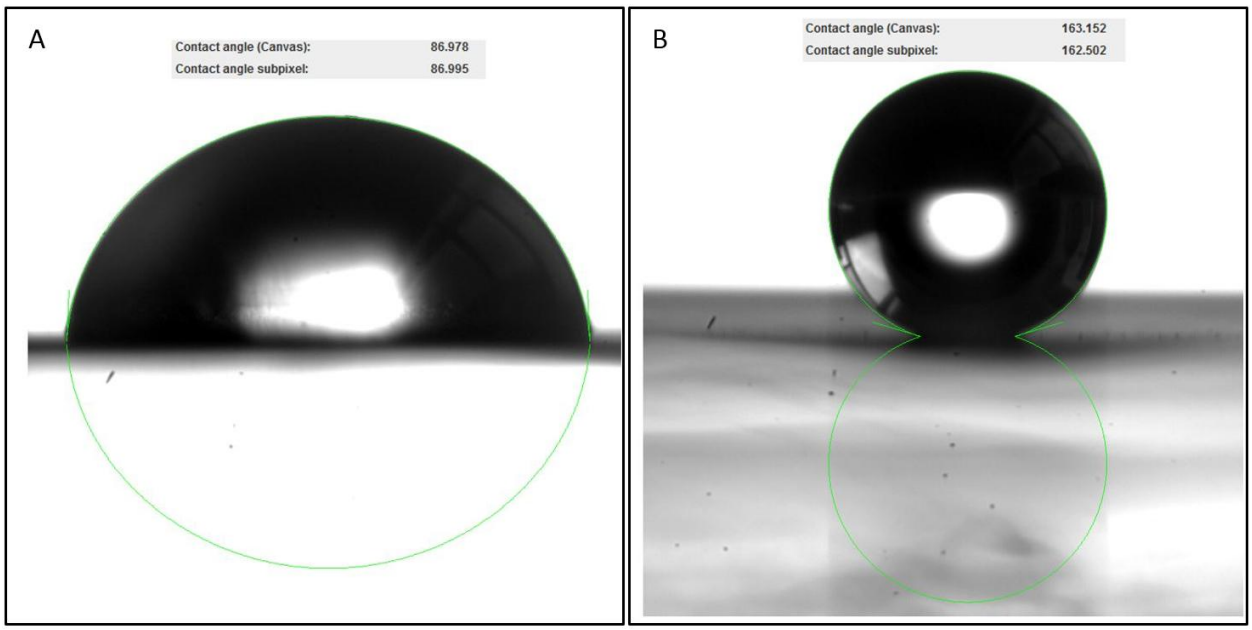

Figure 6. Contact angle between a 2μL water droplet and (A) the Cu substrate, (B) the black NiO film.

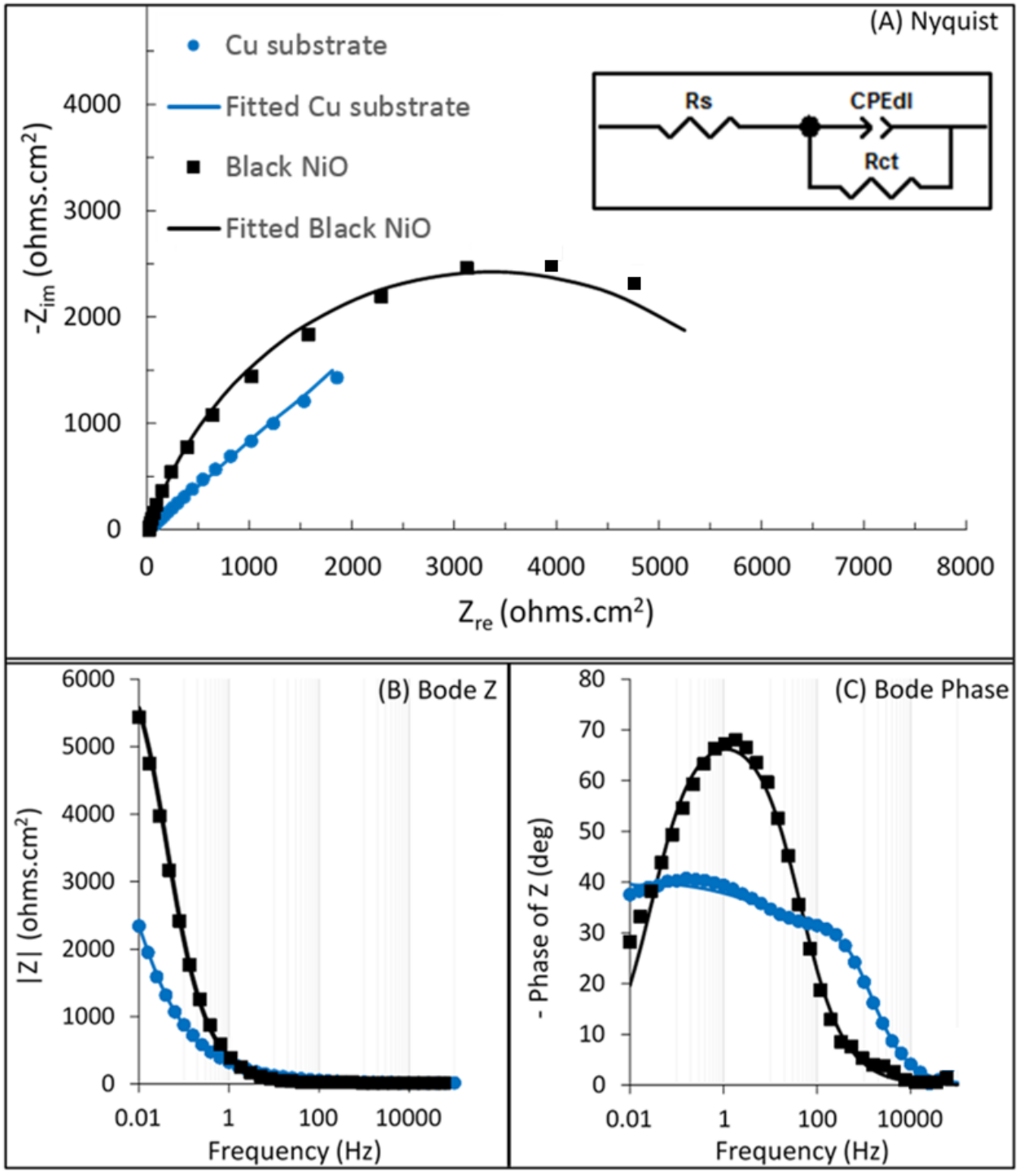

Figure 7. (A) Nyquist, (B) bode Z, and (C) bode phase plots of the black NiO film and the Cu substrate.

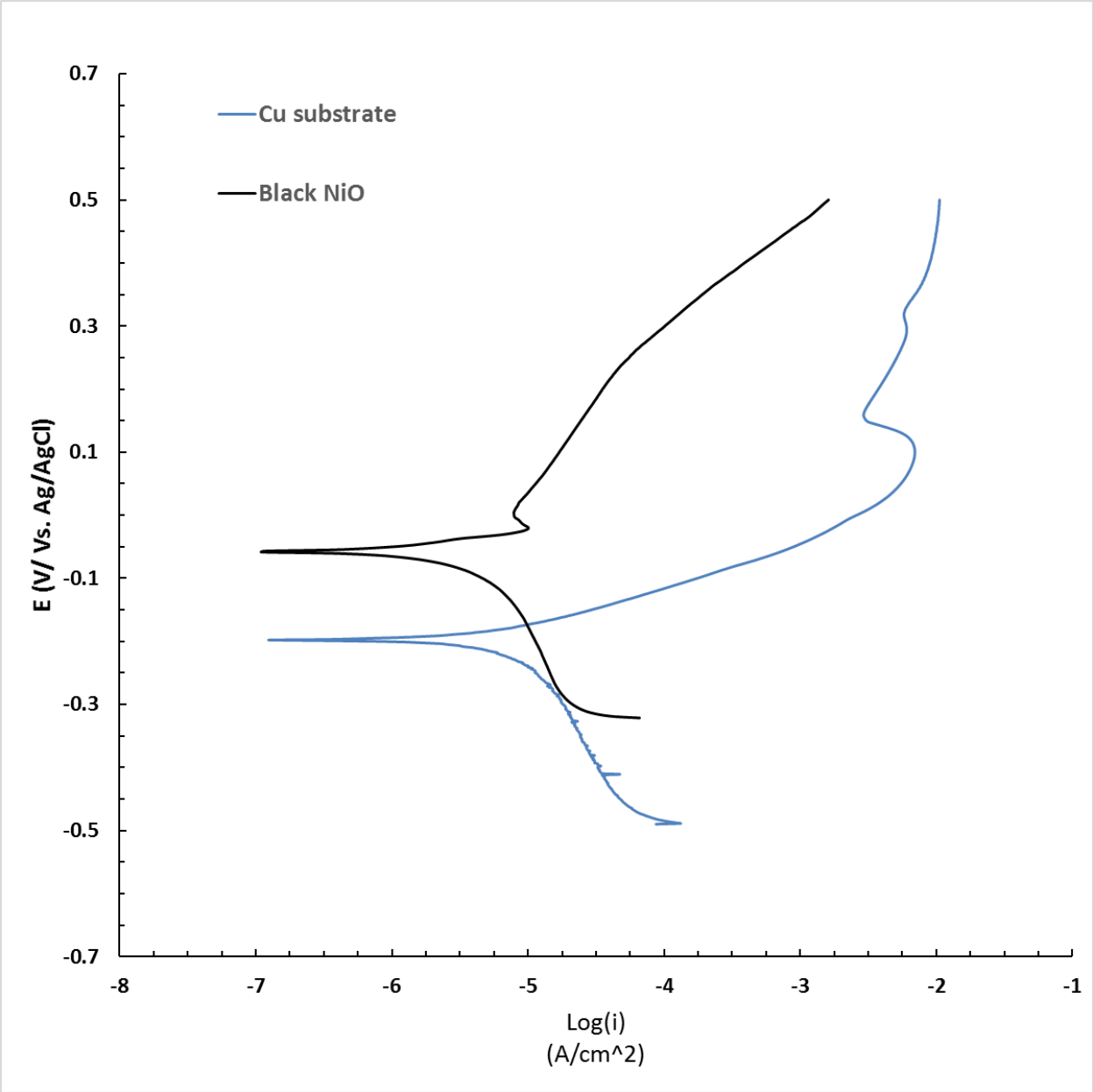

Figure 8. Tafel plots of the black NiO film and the Cu substrate.

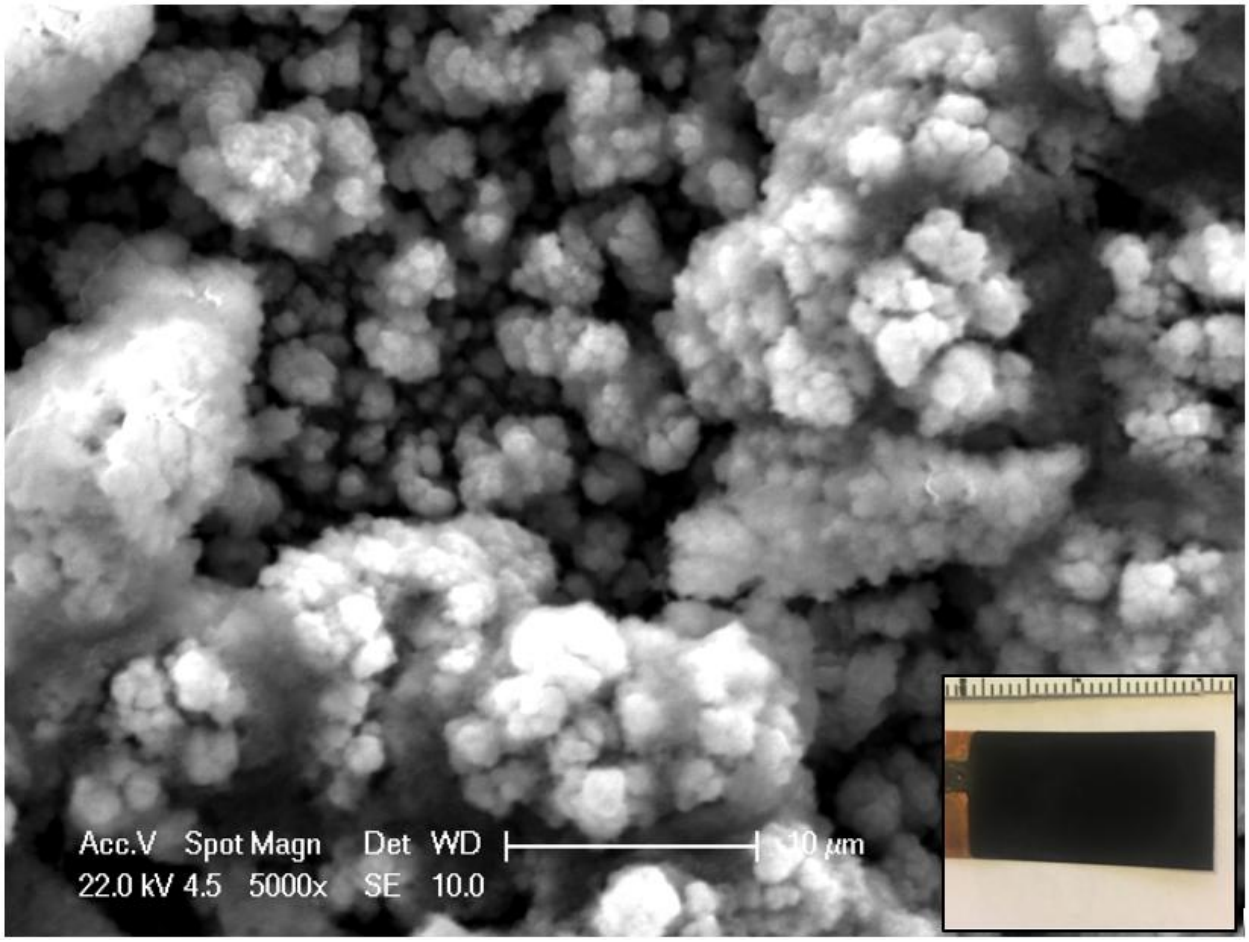

Figure 9. The general aspect and surface morphology of the black NiO film after the corrosion tests.